Switching Capacitor Strategy for fully exploiting potential of EMI filters

Anyu Wang[1], Feng Zheng[1], Zhiqiang Wang[1] and Tian Gao[1]
[1] Xidian University, China

***Abstract*-- In DC/AC inverter systems, the saturation of the common mode (CM) inductor caused by common mode voltage is an important issue in electromagnetic interference (EMI) filter design. Especially for off-the-shelf EMI filter products, the CM voltages, switching frequency, modulation strategy and CM path impedance are often unknown, which is more likely to cause core saturation due to CM path resonance. Although the saturation issues can be avoided by increasing the design margin of magnetic cores, they are often unacceptably expensive in high-power systems. This paper proposes a capacitor adjustment strategy for preventing saturation of CM choke which is suitable for general EMI filters. The principle is to make the filter corner frequency far away from the switching frequency of inverters. The cost of proposed strategy is low. It only needs to detect the volt-seconds on the CM chokes to adjust the number of the connected Y capacitors.**

***Index Terms*--Magnetic cores, Filters, Electromagnetic compatibility, Capacitance.**

I. Introduction

Voltage source inverters (VSI) bring the electromagnetic interference (EMI) issues in motor drive systems [1]. Hence, the CM filters are ubiquitously applied in these systems to effectively attenuate the CM current. Usually, CM EMI filters can take up to 25% the system volume. CM filters will lose their attenuation capability in case CM choke encounter core saturation problem [1]. Although overdesigning the magnetic component is a safe way to prevent the core from saturation, this will lead to an undesirable bulky EMI filter.

Recently, some researchers have discussed the CM choke saturation issues caused by CM voltage. Fang Luo addressed that the CM voltage / CM volt-second can actually determine the CM flux density of CM chokes, and cause the CM chokes to be saturated. In addition, his research results revealed that the volume of the CM choke will significantly increase when the corner frequency fc of EMI filters is close to switching frequency f_{sw} of the inverter. In order to reduce the volume of filters, Bilel Zaidi proposed an optimization method on the design of a toroidal CM inductor with taking magnetic core saturation issues into consideration [2]. Henglin Chen proposed a method to suppress the self-resonance of the low frequency (LF) CM path, which can deal with the saturation problem of the CM choke [3]. However, methods mentioned above are all anti-saturation methods for specific systems. Engineers have to measure, simulate, and extract all CM path parameters to complete the filter design[4].

For off-the-shelf EMI filters, it is difficult to design CM chokes accurately because connected systems are different and unknown. The saturation may cause serious damage and bring huge cost losses. High power universal commercial EMI filters often only specify rated voltages and currents, and don't indicate parameters such as applicable inverter switching frequency f_{sw}. Therefore, for users, the saturation of these filters due to self-resonance is unpredictable and the high cost is unbearable.

In order to avoid CM chokes saturation issues of off-the-shelf EMI filters, this paper proposes an autonomous adjustment strategy by changing Y capacitance. To simplify the required hardware equipment as much as possible, the proposed method only needs to detect the volt-second on the CM choke as the judgment basis of switching Y capacitors. As a result, the off-the-shelf EMI filters can be protected from saturation and the application range of an off-the-shelf EMI filter can be expanded.

In section II, a DC-fed motor drive system with a CM *LCL* filter is taken as an example to demonstrate the principle. In section III, the switching strategy is described. In section IV, the experimental results show saturation issues of inductors are improved by proposed strategy.

II. Analysis of Volt-second for CM Inductors

A. CM equivalent path of DC-Fed Motor Drive Systems

A motor drive system with a *LCL* type CM filter is shown in Fig. 1, where C_y, C_{sc} and C_{sh} are the CM capacitor of the filter, the stray capacitance between the motor windings and chassis, and the stray capacitance between the power module and the heatsink, respectively. At the same time, the Line Impedance Stabilization Network (LISN) is installed in the DC power line. The motor drive system adopts the sinusoidal pulse width modulation (SPWM) whose switching frequency f_{sw} is 10 kHz. In order to attenuate the switching noise and effectively suppress the CM noises current flowing through the motor, a *LCL* filter is connected between the motor and the inverter. As presented in [4], balancing the inductance of the two inductors of the *LCL* filter, namely $L_{cm1} = L_{cm2}$, will lead to the minimal overall filter volume.

The propagation paths of conduction CM noises shown in Fig. 1 can be equivalent to a two-port network as shown in Fig. 2. Since the saturation of the CM chokes will mainly occur near the switching frequency, the discussion will be carried out within this range. On the left hand side of the noise source V_{cm}, the impedance of C_{sh} is much larger than that of LISN. Hence, neglecting it will lead to little error to the analysis results. While, the impedance of

C_{sc} is much larger than R_m and L_m. The CM impedance of the motor can then be equivalently represented by a capacitor.

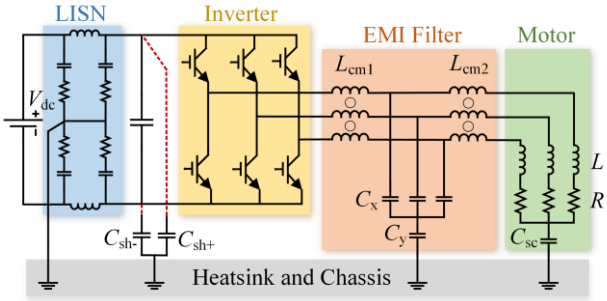

Fig. 1 Motor drive with an *LCL* CM filter

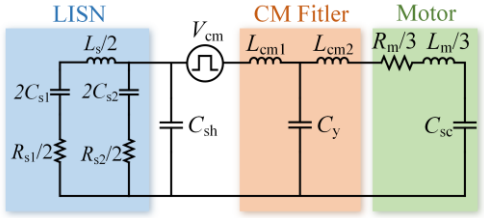

Fig. 2 Equivalent CM path for motor drive system.

The volt-second product on the CM chokes determines the flux density of the magnetic core. The waveform of V_{cm} is shown in Fig. 3 in blue curve. In order to simplify the analysis, a sinusoidal waveform with the same voltage-second product is shown in Fig. 3 in orange. The frequency of V_{sin} is equal to switch frequency f_{sw} and its amplitude is given by (1).

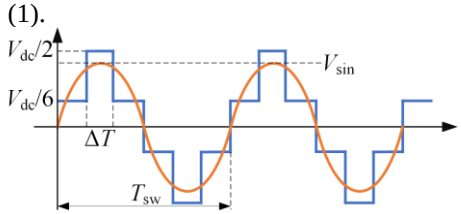

Fig. 3 Equivalent sinusoidal signal with CM voltage V_{cm}.

$$V_{sin}=\frac{\pi}{2}\frac{2\Delta T\left|(1/2)V_{dc}\right|+(T_{sw}-2\Delta T)\left|(1/6)V_{dc}\right|}{T_{sw}} \quad (1)$$

where V_{dc} is the DC voltage and $T_{sw} = 1/f_{sw}$. Finally, the CM model illustrated in Fig. 4 is obtained.

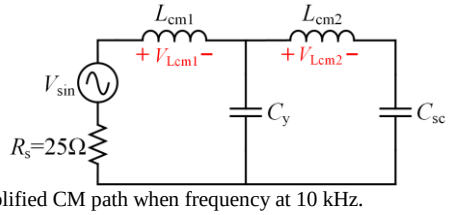

Fig. 4 Simplified CM path when frequency at 10 kHz.

B. Relationship between saturation and CM capacitors

The max flux density B_s of a magnetic core of a CM choke with sinusoidal excitation is determined by

$$B_s=\frac{\left|\dot{V}_{Lcmx}\right|}{2\pi f_{sw}NA_e} \quad (2)$$

where V_{Lcmx} is the voltage across L_{cm1} or L_{cm2}, N is the winding number of turns, and A_e is the cross-sectional area of the magnetic core. Clearly, the flux density is proportional to the voltage across L_{cm1} or L_{cm2} for a given design.

C_y will affect the voltage across the inductors. Taking C_y in Fig. 4 as an independent variable, the voltage gains of L_{cm1} and L_{cm2} can be expressed as

$$G_1(C_y)=\frac{V_{Lcm1}}{V_{sin}}=\frac{(\omega_{sw}^4L^2C_{sc}+1)C_y+C_{sc}}{K_1C_y+K_2} \quad (3)$$

$$G_2(C_y)=\frac{V_{Lcm2}}{V_{sin}}=\frac{-\omega_{sw}^2LC_{sc}}{K_1C_y+K_2} \quad (4)$$

where

$$\begin{aligned}K_1&=\omega_{sw}^4L^2C_{sc}-j\omega_{sw}^3R_sLC_{sc}-\omega_{sw}^2L+j\omega_{sw}R_s\\K_2&=j\omega_{sw}R_sC_{sc}-2\omega_{sw}^2LC_{sc}+1\\L&=L_{cm1}=L_{cm2}\end{aligned} \quad (5)$$

Assume the value of L is 4.8mH, and C_{sc} is 0.1nF, 0.4nF and 1.6nF, respectively. Fig. 5 shows voltage gain of two inductors when C_y varies from 100pF to 10μF. The following conclusion can be drawn by reading Fig. 5.

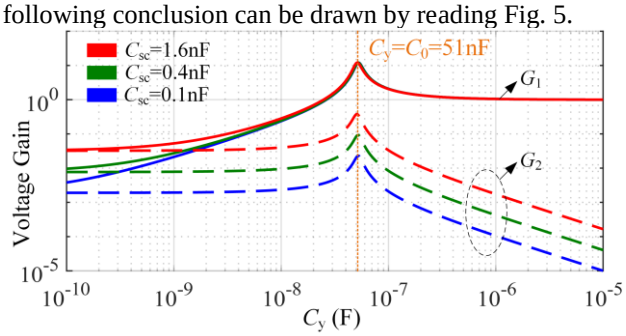

Fig. 5 When C_{sc} is 0.1, 0.4, and 1.6nF, the voltage Gain of L_{cm1}, L_{cm2}.

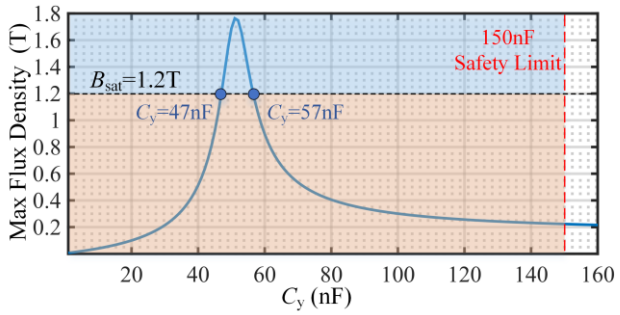

Fig. 6 V_{sin} =7V, N = 10, A_e = 76 mm^2, calculated B_s in nanocrystalline core.

When $C_y = C_0$ (the filter corner frequency f_c is close to the switching frequency f_{sw}), the voltage amplitudes of the two inductors increase significantly. This is consistent with the views before.

When L_{cm1} and L_{cm2} are the same, V_{Lcm1} will be always greater or equal than V_{Lcm2}. This means that as long as the L_{cm1} is unsaturated, the L_{cm2} will not be saturated.

The following case will be taken to demonstrate our idea. In this case, CM inductors are fabricated with a nanocrystalline core. Assume N is 10 and A_e is 76 mm^2. The amplitude and frequency of the sinusoidal CM voltage excitation V_{sin} is 7 V and 10kHz, respectively. The relationship between the B_s and C_y is demonstrated in Fig. 6. The L_{cm1} will only be saturated when the value of C_y is located in the interval from 47nF to 57nF. Hence, if the C_y can be adjusted in real-time, the saturation caused by self-resonance of CM path will be avoided.

III. Capacitor Adjustment Strategy

A. The principle of capacitor adjustment

The switching frequencies f_{sw} of VSI will vary from case to case. An off-the-shelf EMI filter should be adapted to these different cases as much as possible. From section II can we know, if an off-the-shelf EMI filter is saturated, this does not mean that an EMI filter with greater power rating must to be purchased. Instead, adjusting the C_y to make f_c deviate from f_{sw} will make an filter more widely applicable. The capacitance C_y can be controlled by adjusting the number of connected capacitors. There are 3 principles of proposed adjusted strategy:

1) The upper limit of C_y is the safety regulations. It depends on leakage current and safety standards. This letter takes 150nF as the upper limit.
2) The lower limit of C_y is zero.
3) Making C_y close to the upper limit as much as possible with keeping the CM chokes unsaturated. This is to achieve more insertion loss under unsaturated condition.

In a volt-second product fixed system, the characteristic of B_s vs C_y is invariable. It can be classified into five cases as shown in Fig. 7. As shown in Fig. 7 (a), (b) and (c), the best capacitance C_y is 150nF, which reaches the safety limit. As shown in Fig. 7 (d), the best C_y makes the inductor critically saturated. As shown in Fig. 7 (e), it is indicated that the power rating of the filter is too small to fit the system, and it is necessary to stop working and replace the filter. In summary, the capacitance adjustment strategy should automatically find the best for each case.

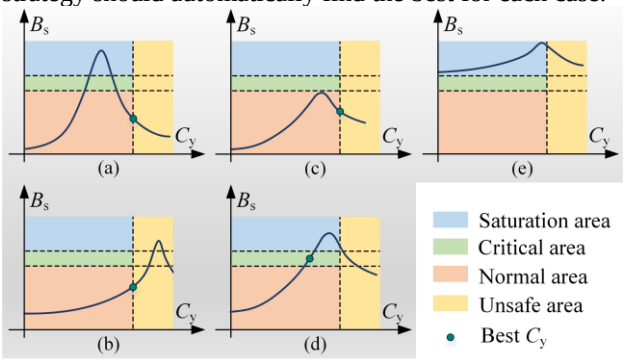

Fig. 7 Five cases between B_s and C_y for a volt-second fixed system.

B. Variable switching frequency and volt-second

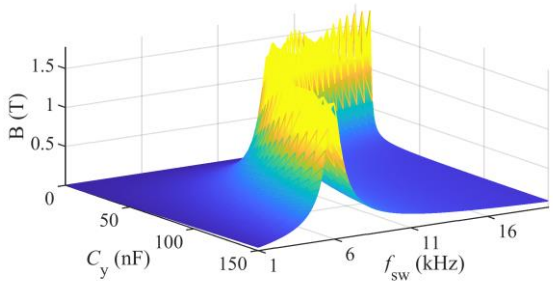

Fig. 8 Trend of flux density with switching frequency.

In practical applications, the switching frequency and volt-second value of an inverter may vary[5-7]. Whenever the switching frequency or the volt-second changes, the characteristic of B_s vs C_y will also change accordingly. Fig. 8 shows the variation trend of magnetic flux density of cores with different switching frequency f_{sw}. It can be observed that even in the same system, changes in the switching frequency will lead to changes in the optimal Y capacitance. Therefore, how to continuously find the optimal number of Y capacitors in a dynamic system is the topic of this section.

When the switching frequency or modulation degree changes, the characteristic curve of B_s vs C_y will change from one state to another. Excluding the case of exceeding the rated power shown in Fig. 7 (e), the changes of the curves can be classified into 4x4 categories, as shown in Fig. 9. In each figure, the solid line represents the initial state, and the dashed line represents the case after the change in state.

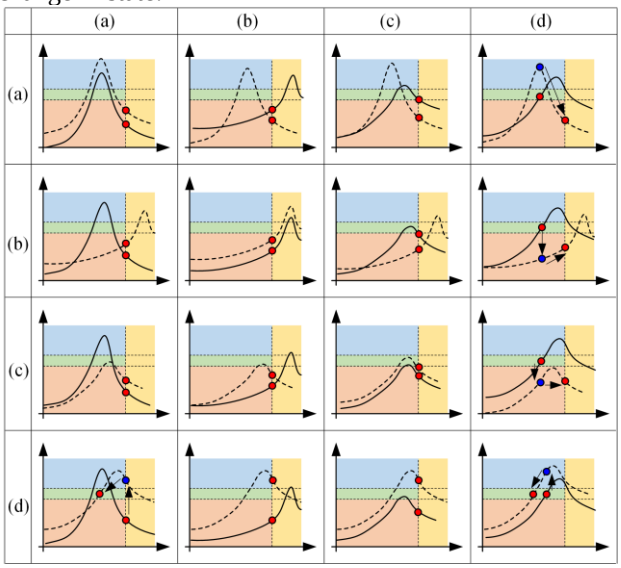

Fig. 9 The characteristic curve of B_s vs C_y.

The mutual transformation of the three cases, (a), (b), and (c), makes no difference to the capacitance adjustment strategy. Because the optimal number of Y capacitors has all reached the safety standard limit. The situation that requires dynamic adjustment of Y capacitors is related to case (d). The only measure of the proposed method mentioned in this paper is the magnetic flux density of the magnetic ring. Therefore, it can be divided into two situations: detecting an increase in magnetic flux density and detecting a decrease in magnetic flux density.

If detecting an increase in magnetic flux density, there are two possibilities:

1) It is shown in Fig. 10. The initial state is at point A. With the increase of switching frequency, the B_s vs C_y curve changes and the state becomes A_1. At this time, the adjustment strategy needs to increase the number of Y capacitors to transform the state from point A_1 to point A_2 to prevent saturation.

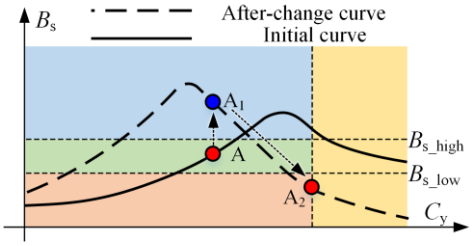

Fig. 10 When detecting an increase in magnetic flux density.

2) As shown in Fig. 11, the initial state is at point B. With the decrease of switching frequency, the curve of B_s vs C_y changes and the state becomes B_1. At this time, it is necessary to reduce the number of Y capacitors to transform the state from B_1 to B_2.

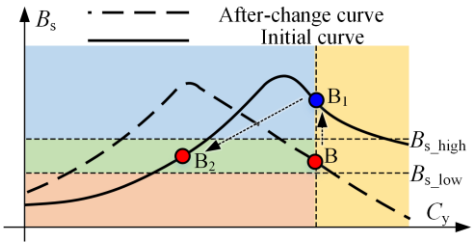

Fig. 11 When detecting an increase in magnetic flux density.

If detecting an decrease in magnetic flux density, as shown in Fig. 12. Since the CM inductor is away from saturation, the number of Y capacitors can be increased to achieve a higher insertion loss.

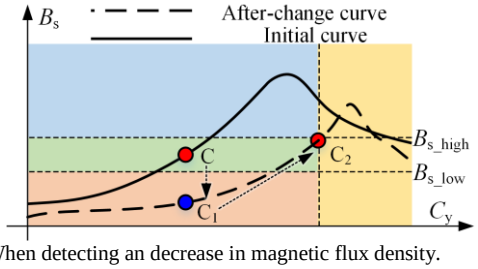

Fig. 12 When detecting an decrease in magnetic flux density.

In summary, when an increase or decrease in magnetic flux density is detected, it is impossible to determine whether the number of Y capacitors should be increased or decreased. Therefore, the capacitor adjustment strategy proposed in this paper is to achieve real-time adjustment in the variable volt-second system by increasing the number of Y capacitors one by one.

The block diagram of the control strategy is shown in Fig. 13. First, connect all capacitors (150nF) and detect B_s to determine whether the inductor L_{cm1} is saturated. If L_{cm1} isn't saturated, it indicates case (a), (b) or (c), and at this time 150nF is the best. At this time, the block diagram executes in loop 1. If L_{cm1} is saturated, it indicates case (d) or (e), and at this time it should disconnect all capacitors to prevent L_{cm1} from continuing to saturate.

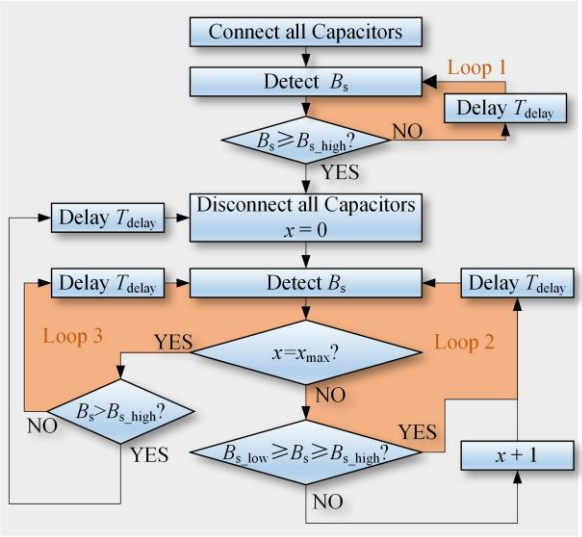

Fig. 13 Block diagram of the adjustment strategy.

After disconnecting all capacitors, increase the number of Y capacitors one by one until the magnetic flux density is between B_{s_low} and B_{s_high}. At this point, the program enters loop2 to loop. As the operating conditions continue to change, when the number of Y capacitors reaches the upper limit again and the inductor is not saturated, the program enters Loop3 to loop. If it is still saturated at this time, it is necessary to disconnect all Y capacitors and add them one by one again to find a new optimal point. In order to prevent unexpected ringing, every capacitor switching need to wait for T_{delay} after the previous action. If a full cycle fails to find the optimal point, it is indicated that the power rating of the filter is too small to fit the system. And the system should be shut down.

IV. Experimental Results

A. Verify the Y capacitor adjustment strategy

To validate the proposed method, we use the circuit and component parameters shown in Fig. 14 to represent the CM path of the motor drive system. An integrator is used to measure the volt-second production of L_{cm1}. The control scheme is fulfilled by a DSP control card. The square waveform voltage source V_{inv} is with the same frequency and volt-second product as V_{cm}. The voltage source is generated by a single-phase inverter, which switch frequency f_{sw} is 10kHz. The experiment setup is illustrated in Fig. 15. The 1.87mH inductor L_{cm1} and L_{cm2} are fabricated using a nanocrystalline core, T60006-L2030-W358, with 11 turns. The saturation flux density is 1.2T and the cross-section area of magnetic core is 40 mm^2. The switching capacitors array is composed of ten 15nF capacitors.

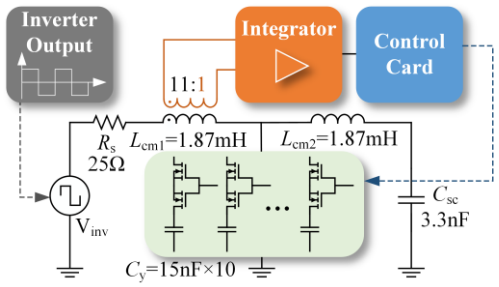

Fig. 14 Experimental system structure;

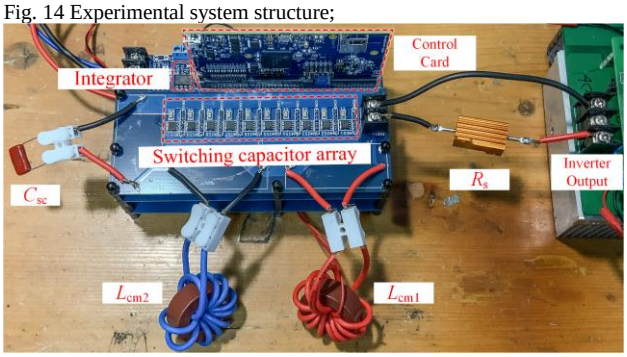

Fig. 15 Experimental system structure;

Fig. 16 shows the time domain waveform of experimental result when the connected capacitance is 0nF, 45nF, and 105nF. As shown in Fig. 16 (b) and (c), the volt-second on L_{cm1} varies greatly. Using the peak voltage of the integrator output, V_{inter_peak}, shown in Fig. 16 (c), the max flux density B_s of L_{cm1} is given by (6).

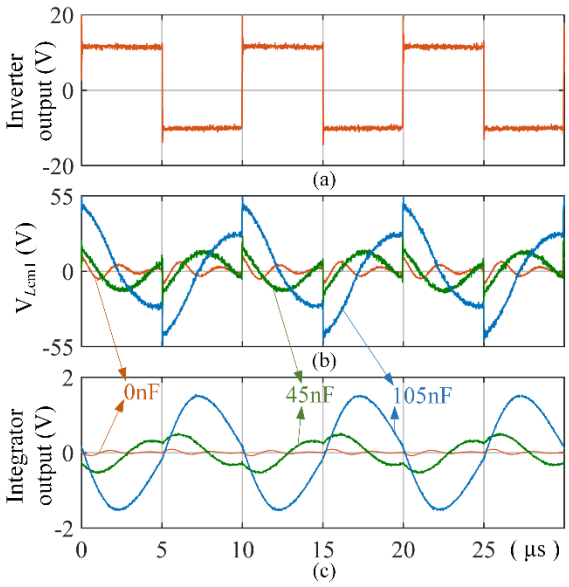

Fig. 16 When V_{inv} = 10V, (a)Inverter output voltage; (b)Voltage of L_{cm1}; (c)voltage of integrator output.

$$B_s = 0.825 \times V_{inter\_peak} \quad (6)$$

The max flux density B_s of L_{cm1} with different capacitances are measured when V_{inv} is 5V, 10V and 15V, respectively. The experimental results are shown in Fig. 17. No matter what C_y being, the L_{cm1} will not saturate when V_{inv} is 5V. In this case, the best capacitance is 150nF. When V_{inv} is 10V and 15V, 150nF capacitance will make L_{cm1} saturated. So the best capacitance is then 75nF and 60nF, respectively.

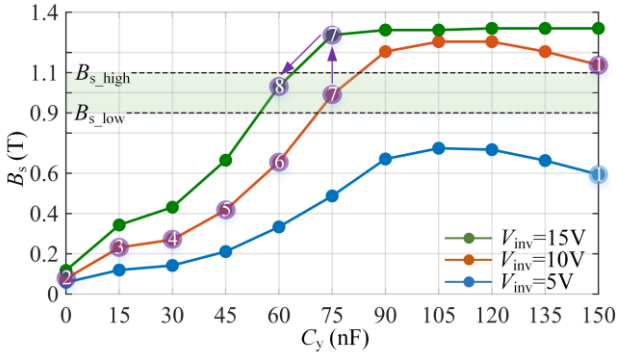

Fig. 17 When V_{inv} = 5V,10V,15V, measured B_s with C_y = 0~150nF. When V_{inv} is always 5V, the adjustment strategy is only step ①; When V_{inv} changes from 10V to 15V, the adjustment strategy are step ① to ⑧.

In order to verify the adjustment strategy, we set two working conditions.

a) The V_{inv} keep stable at 5V. In the experiment the number of connected capacitors is always 10. The only one step is shown in Fig. 17 in the blue circle 1.

b) The V_{inv} is initially 10V and suddenly change to 15V at 1 minute. At the beginning, 10 capacitors are connected. Then the connected capacitances change in the sequence of 150nF, 0nF, 15nF, 30nF, 45nF, 60nF, and 75nF. When the suddenly change is applied, the connected capacitances decrease from 75nF to 60nF. The above steps are carried out in the order of the purple circle number in Fig. 17. This indicates the best capacitance under 10V excitation is 75nF. As the volt-second increase, the controller can successfully maintain the proper working condition of the inductors by reducing the number of capacitors to 60nF.

B. Verification of adaptive filter prototype

To further verify the effectiveness of the proposed capacitors adjustment strategy, a prototype EMI filter with an apparent power of 60 kW was fabricated in this study, as shown in Fig. 18. The blue PCB includes a volt-second detection circuit, a control circuit, and adjustable Y capacitors. The number of connected Y capacitors is controlled by the relay. The right of Fig. 18 shows the exploded view of the complete EMI filter. The CM inductor is composed of copper bars and nanocrystalline oval rings. The adjustable capacitor PCB board is connected to the common-mode inductor via bolts to form an LC topology.

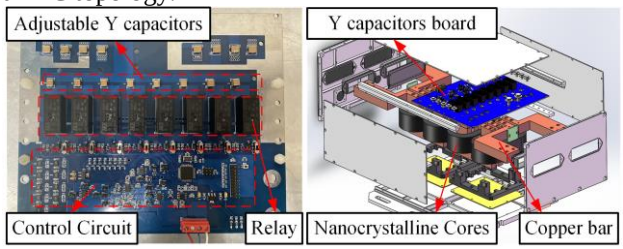

Fig. 18 The prototype of adaptive EMI filter.

To verify the performance of the filter, the experimental setup shown in Fig. 19 was used.

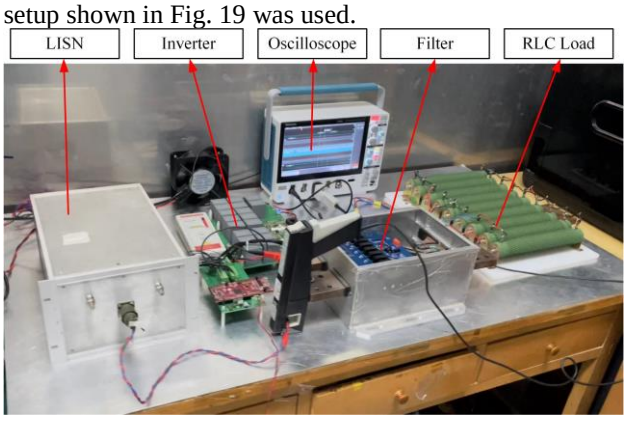

Fig. 19 The experimental equipment.

The DC input voltage is 350V. The switching frequency is 15kHz.The inverter is implemented by the FS800R07A2E3 IGBT power module produced by Infineon. RLC is used in series as the load of the inverter, and its maximum power capacity is 10 kW. The EMI filter prototype is connected between the LISN and the DC input side of the inverter. The voltage and current time-domain waveforms are measured using Tektronix's MOD34 series oscilloscope. The CM noise is measured using Rohde & Schwarz's FPL1003 spectrum analyzer.

In order to observe the state of the filter when it is saturated due to resonance in the system, the first step of this experiment is to disable the adaptive adjustment function of the filter and test the online impedance of the CM inductor. By performing FFT operations on the voltage and current on the CM inductor, the frequency domain impedance of the CM inductor can be obtained. The impedance of CM inductor after saturation is shown in Fig. 20 blue curve. Then turn on the function of adaptive adjustment. Measure the CM voltage and CM current on

the CM inductor after adjustment. And calculate the impedance of the common-mode inductor at this time, as shown in the red line in Fig. 20.

It can be found that without the adaptive function turned on, the CM inductance will experience impedance reduction due to saturation. Especially in the low frequency range, the impedance of the saturated CM inductor is much lower than that of the unsaturated case.

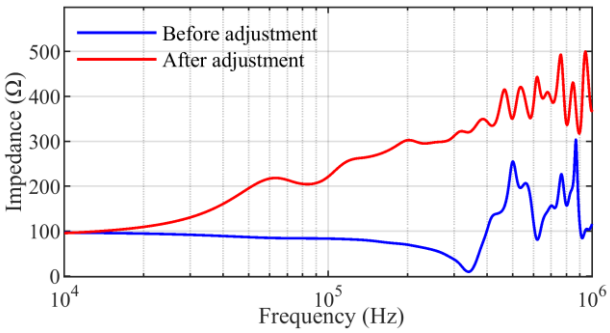

Fig. 20 Measurement of CM inductance impedance.

In addition, by calculating the measured CM voltage and CM current, the hysteresis loops under two conditions can be obtained as shown in Fig. 21. It can be seen that the adaptive method changes the CM inductance from a saturated state to a non-saturated state. Before adjustment, the magnetic flux density in the magnetic core had reached a maximum of around 1.2T, which confirms that the impedance drop in the blue line in Fig. 20 was caused by saturation. After adaptive adjustment, the maximum magnetic flux density dropped to around 0.9T. At this point, the magnetic core is within a safe operating range, achieving the goal of adaptive adjustment.

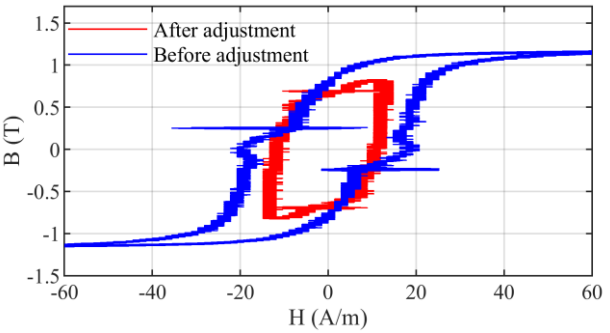

Fig. 21 Measured hysteresis loop.

The CM noise measurement results of the filter prototype are shown in Fig. 22. The green line represents the unfiltered raw noise, while the blue line represents the noise after filtering.

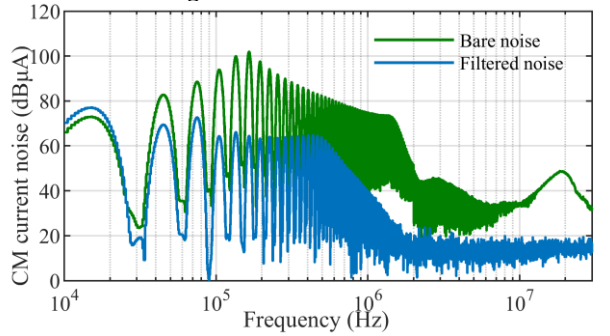

Fig. 22 Measured CM noise currents.

It can be observed that the filter effectively suppresses the noise beyond 150 kHz, which validates the effectiveness of the adaptive adjustment function in controlling the operating state of the CM inductor. This ensures that the filter always operates in the optimal state, thereby improving the versatility of the EMI filter.

V. Conclusions

This paper discussed adjusting the capacitance value can eliminate the CM inductor saturation problem caused by self-resonance. Based on this theory, an adaptive anti-saturation strategy with a simple integrator and capacitors switching device is proposed. Applying the strategy, off-the-shelf EMI filters are able to work normally in systems with different switching frequency or modulation index. For an off-the-shelf EMI filter, although reducing the number of capacitors may attenuate the insertion loss, the goal of the proposed method is to achieve maximum insertion loss on the basis of ensuring safety, which similar to a kind of anti-saturation “fuse”. As a result, the full potential of an off-the-shelf EMI filter is exploited.

References

[1] W. Shen, F. Wang, D. Boroyevich, V. Stefanovic, and M. Arpilliere, "Optimizing EMI filter design for motor drives considering filter component high-frequency characteristics and noise source impedance," in *Nineteenth Annual IEEE Applied Power Electronics Conference and Exposition, 2004. APEC '04.*, 2004, pp. 669-674 vol.2.

[2] B. Zaidi, A. Videt, and N. Idir, "Optimization Method of CM Inductor Volume Taking Into Account the Magnetic Core Saturation Issues," *IEEE Transactions on Power Electronics*, vol. 34, pp. 4279-4291, 2019.

[3] H. Chen, J. Wu, and X. Zheng, "Elimination of Common-Mode Choke Saturation Caused by Self-Resonance of the EMI Filter in a Variable-Frequency Drive System," *IEEE Transactions on Electromagnetic Compatibility*, vol. 61, pp. 1226-1233, 2019.

[4] M. L. Heldwein and J. W. Kolar, "Design Of Minimum Volume Emc Input Filters For An Ultra Compact Three-phase Pwm Rectifier," 2007.

[5] T. G. Habetler and D. M. Divan, "Acoustic noise reduction in sinusoidal PWM drives using a randomly modulated carrier," in *20th Annual IEEE Power Electronics Specialists Conference*, 1989, pp. 665-671 vol.2.

[6] X. Zhao, D. Jiang, Q. Li, Y. Ma, and Y. Liu, "An Application of Variable Switching Frequency PWM on SiC-Based Paralleled Inverters for Motor Drive," in *2020 IEEE 9th International Power Electronics and Motion Control Conference (IPEMC2020-ECCE Asia)*, 2020, pp. 1151-1155.

[7] A. M. Trzynadlowski, K. Borisov, L. Yuan, and Q. Ling, "A novel random PWM technique with low computational overhead and constant sampling frequency for high-volume, low-cost applications," *IEEE Transactions on Power Electronics*, vol. 20, pp. 116-122, 2005.